Dalton Transactions

ROYAL SOCIETY OF CHEMISTRY

PAPER

View Article Online
View Journal | View Issue

Cite this: *Dalton Trans.*, 2022, **51**, 4079

Exploration of metal sulfide syntheses and the dissolution process of antimony sulfide in phosphonium-based ionic liquids†

Matthias A. Grasser,[a] Tobias Pietsch,[a] Eike Brunner [a] and Michael Ruck *[a,b]

Received 10th December 2021,
Accepted 4th February 2022

DOI: 10.1039/d1dt04165g

rsc.li/dalton

Ionic liquids (ILs), especially task-specific ILs, are capable of dissolving various solids at moderate temperatures without the need for special reaction vessels. Direct synthesis of binary sulfides of B, Bi, Ge, Mo, Cu, Au, Sn, In, Ti, V, Fe, Co, Ga, Ni, Al, Zn, and Sb in $[P_{66614}]Cl$ was tested at 100 °C, *i.e.* below the melting point of sulfur. Under these conditions, substantial sulfide formation occurred only for nickel (Ni_3S_4, Ni_3S_2, NiS) and copper (Cu_2S, CuS). Sb showed no formation of crystalline sulfide, but after addition of EtOH, an orange material precipitated which was identified as amorphous metastibnite. Subsequently, the dissolution of antimony sulfide (Sb_2S_3), the main source of antimony production, in the phosphonium-based ILs $[P_{66614}][OAc]$ and $[P_{66614}]Cl$ at 100 °C was studied in detail. The dissolution proceeds without H_2S evolution, and amorphous Sb_2S_3 can be precipitated from these solutions. Heating Sb_2S_3 in the Lewis-acidic IL $[BMIm]Cl{\cdot}4.7AlCl_3$ led to the crystallization of $[Sb_{13}S_{16}Cl_2][AlCl_4]_5$, which contains a new quadruple heterocubane cation.

Introduction

Task-specific ionic liquids (ILs) can dissolve diverse solids (*e.g.* elements, oxides, sulfides) at moderate temperatures, in some cases even at room temperature, without the need for special reaction vessels (autoclave, high-temperature or high-pressure equipment) in normal flasks, making them accessible for downstream chemistry.[1,2] The IL may be a stable and inert solvent or it acts as a reactant that is altered by chemical reaction with the substances to be dissolved.[1–14] Sometimes ions or molecules of the IL are incorporated into the solid products. As a generally less expensive alternative to ILs, deep eutectic solvents (DES) have also been tested for this purpose.[1,4,13,15–19] Of course, large-scale use of ILs or DES only makes sense if they are affordable, are not altered during the reaction, and can be recycled efficiently. Regardless of commercial considerations, a broad knowledge base is required to optimize process parameters for a desired application.

In the following, we focus in particular on the chemistry of antimony sulfide in selected ILs. The ore stibnite (Sb_2S_3) is the main source for antimony production. At contents of 40 to 60%, antimony is obtained by reduction with iron at 550 to 600 °C. From ores with lower contents, the sulfide is roasted to Sb_2O_4 or Sb_2O_3 and then reduced with carbon. The crude antimony obtained usually still contains impurities of sulfur, arsenic, copper, lead and iron.[20] Both pyrometallurgical processes are highly CO_2 and SO_2 emitting. An ecologically and economically viable alternative could be to dissolve the ore and further process the antimony at low temperatures in ILs.[13,21] Such "ionometallurgical" processing of natural resources appears to be a logical, albeit challenging, future application of the known beneficial properties of ILs.

The chemistry of chalcogens and metal chalcogenides in ILs is manifold and gained a lot of interest in recent years.[1,4,6,22–26] Boros *et al.* showed the dissolution of non-metallic solid elements in ILs, in particular the dissolution of sulfur in trihexyltetradecylphosphonium decanoate, $[P_{66614}][dec]$, in which sulfur is highly soluble. The dissolved sulfur species shows a concentration dependency between $[S_3]^{\bullet-}$ and $[S_6]^{2-}$, were the latter one occurs at higher concentrations.[7] In many cases, the IL not only serves as a reaction medium, but parts of it become part of new compounds. Dehnen *et al.*, for example, isolated various thio- and oxothiostannates, selenogermanates and -stannates including cations of the imidazolium-based ILs.[22,23,27–30] Among them, the most prominent compound contains the supersphere anion $[Ge_{24}Sn_{36}Se_{132}]$.[24–31,32] But also a new modification of $K_2Sn_2S_5$ was accessible, which obviously does not include the IL used.[33]

Binary metal chalcogenides, such as the technologically important tetradymite-type compounds Bi_2Ch_3 (Ch = Se, Te),

[a]*Faculty of Chemistry and Food Chemistry, Technische Universität Dresden, 01062 Dresden, Germany. E-mail: michael.ruck@tu-dresden.de*
[b]*Max Planck Institute for Chemical Physics of Solids, Nöthnitzer Str. 40, 01187 Dresden, Germany*

†Electronic supplementary information (ESI) available. CCDC 2125501. For ESI and crystallographic data in CIF or other electronic format see DOI: 10.1039/d1dt04165g

were synthesized as nanoparticles in 1-butyl-3-methylimidazolium iodide [BMIm]I,[34] by Schulz *et al.*,[34–36] Schmidt *et al.*[37,38] and Cademartiri *et al.*[39] Schulz *et al.* also synthesized the promising thermoelectric material Sb_2Te_3 in ILs.[40,41]

The crystallization of homonuclear chalcogen polycations, such as Te_4^{2+},[42–44] or of various antimony-selenium[45–48] and antimony-sulfur[49] heteropolycations succeeded from Lewis-acidic ILs [BMIm]X·$n$$AlX_3$ (X = Cl, Br; n = 1.2–5.2) or 1-ethyl-3-methylimidazolium bromide [EMIm]Br-$AlCl_3$ mixtures. In these cases, halogenidoaluminates are the typical counter ions. Reacting Bi_2S_3 in such ILs led to similar compounds[50–52] but also to the discovery of a molecular form of Bi_2S_3.[50]

Here we present a study on the reactivity of elemental sulfur with various elements in the commercially available IL trihexyltetradecylphosphonium chloride [P_{66614}]Cl at 100 °C aiming at the synthesis of binary sulfides. In the course of these experiments, we discovered that Sb_2S_3 is soluble in phosphonium-based ILs, which we investigated in more detail. Switching to the imidazolium-based IL [BMIm]Cl·4.7$AlCl_3$, led to the crystallization of the new cluster compound $[Sb_{13}S_{16}Cl_2][AlCl_4]_5$.

Results and discussion

Reacting metals with sulfur in [P_{66614}]Cl at 100 °C

We first attempted the controlled synthesis of sulfides of main group and transition metals starting from the elements. As IL, [P_{66614}]Cl was chosen because the commercially available product can be purified[10] and it had already demonstrated good solvent properties in the synthesis of metal phosphides,[8] selenides,[14,53–55] and tellurides.[10] The following elements were tested: B, Bi, Ge, Mo, Cu, Au, Sn, In, Ti, V, Fe, Co, Ga, Ni, Al, Zn, Sb. In a 16-hour reaction at 100 °C, *i.e.*, below the melting point of elemental sulfur (119.6 °C),[56] sulfur readily dissolved but significant sulfide formation occurred only for nickel and copper (Table 1).

The reaction of sulfur with ground nickel powder in the IL resulted in the formation of NiS, Ni_3S_4 and Ni_3S_2 (Fig. S1†). Due to surface passivation by sulfide formation, unreacted nickel was still present after the reaction.

The reaction of equimolar amounts of copper and sulfur in the IL resulted in the formation of CuS. At a molar ratio of the starting materials of 2 : 1, $Cu_{2-x}S$ was obtained (Fig. S2†). When copper was used in the form of flakes, complete conversion to the sulfide was not achieved within 16 hours. Even when the ILs trihexyltetradecylphosphonium acetate [P_{66614}][OAc] or trihexyltetradecylphosphonium dicyanamide [P_{66614}][DCA] were used, in which sulfur has a higher solubility (2 equivalents of sulfur dissolve in [P_{66614}][OAc] at 100 °C as a stable solution), residuals of copper were observed in the PXRD or macroscopically as flakes. In contrast to the synthesis in the chloride IL, where the reaction mixture had a yellow color even before stirring, the acetate IL produced a red color directly around the sulfur, which changed to turquoise when diluted into the IL. Boros *et al.* had reported similar colors for the dissolution of sulfur in [P_{66614}][dec] and had attributed them to $[S_6]^{2-}$ (red) and $[S_3]^{\bullet-}$ (blue).[7] It seems that sulfur partially disproportionates in [P_{66614}][OAc] and [P_{66614}][DCA], while only uncharged S_8 molecules are present in [P_{66614}]Cl. A parallel observation was recently made for tellurium in the same phosphonium-based ILs.[57,58] With stirring and heating, the acetate IL darkened completely to a dark red to brownish solution at a molar ratio of Cu : S = 1 : 1, and a dark green solution was formed for 2 : 1.

The reaction of antimony and sulfur in [P_{66614}]Cl or in [P_{66614}][OAc] at 100 °C for 16 h gave a grayish solid with a yellow to orange IL supernatant (see below). The light yellow acetate IL turned green at the beginning of the reaction, which we assign to the intermediate formation of the blue radical anion $[S_3]^{\bullet-}$. Apparently, the IL favors bond breaking in S_8 molecules. After removing most of the IL with a pipette and washing with ethanol (EtOH), a gray solid with some traces of an orange phase remained (see below). The gray solid was identified by powder X-ray diffraction (PXRD) as unreacted antimony (Fig. S3 and S9†).

Dissolution of antimony sulfide in [P_{66614}]Cl and [P_{66614}][OAc]

Since Sb_2S_3 appears to be somewhat soluble in phosphonium-based ILs, we followed up on this observation. Freshly ground crystalline Sb_2S_3 was heated to 100 °C in dried or additionally purified [P_{66614}]Cl or [P_{66614}][OAc] under vigorous stirring. This resulted in a color change of the IL, from colorless to green for the chloride and from light yellow to yellow-green for the acetate, similar to the reaction of the elements described above. The solubility in general was relatively low, below 1 wt%. Raman spectra of the solutions, after separation from undissolved starting material, showed no signals of Sb–S, S–S, or Sb–Sb bonding modes (Fig. S4 and S5†). Cyclic voltammetry (CV) of the solution (Fig. S6†) showed only reversible hysteresis and no discrete peaks, indicating no redox reactions in the range from −3.5 V to 3 V. There was not much difference between purified and unpurified ILs. Nevertheless, Sb_2S_3 could be precipitated from the filtered solutions (see below), which is a strong indication of the mobilization of Sb_2S_3 by the selected phosphonium-based ILs.

We used ^{1}H-, ^{13}C- and ^{31}P-NMR spectroscopy to check whether the ILs were chemically altered by the reaction. All

Table 1 Successful reactions of metals with elemental sulfur in phosphonium-based ILs at 100 °C. B, Bi, Ge, Mo, Au, Sn, In, Ti, V, Fe, Co, Ga, Al, and Zn did not react

Starting materials	IL	Sulfides formed
Ni + 2S	[P_{66614}]Cl	NiS, Ni_3S_4, Ni_3S_2 [a]
Cu + S	[P_{66614}]Cl	CuS[b]
	[P_{66614}][OAc]	$Cu_{2-x}S$[b]
2Cu + S	[P_{66614}]Cl	$Cu_{2-x}S$[b]
	[P_{66614}][OAc]	$Cu_{2-x}S$[b]
2Sb + 3S	[P_{66614}]Cl	Traces of amorphous Sb_2S_3 after addition of EtOH[c]
	[P_{66614}][OAc]	

[a] Detailed PXRD pattern in Fig. S1.† [b] Fig. S2.† [c] Fig. S3.†

spectra recorded after solvation fit very well with the spectra before. We conclude that the IL did not decompose under the given conditions and that there are no strong interactions between the cation of the IL and the dissolved species (Fig. S7 for $[P_{66614}]Cl$ and Fig. S8† for $[P_{66614}][OAc]$). Thus, $[P_{66614}]Cl$ supports Sb–S bond breaking in crystalline Sb_2S_3 without being affected by any chemical reaction itself. As the IL proves to be a chemically and thermally stable solvent it can be recycled.

Amorphous antimony sulfide from ILs

As mentioned above, the reaction of antimony and sulfur in $[P_{66614}]Cl$ or in $[P_{66614}][OAc]$ at 100 °C gave a yellow to orange solution. The addition of *ca.* 3 mL dichloromethane (DCM) to 1 g of the solution resulted in an orange dispersion. Using ethanol (EtOH) as solvent resulted in an orange, bulky powder that deposited over hours. The powder was very voluminous, but in the course of precipitation and drying it collapsed. From 5 mL solution about 5 mg of powder could be precipitated. Similarly, a yellow to orange solid precipitated from the colored solutions obtained by dissolving Sb_2S_3 in $[P_{66614}]Cl$ or $[P_{66614}][OAc]$ in air. The process started after 5 minutes at the surface, but it took weeks to completely decolorize the IL. The addition of EtOH accelerated the process.

Characterization of the precipitates revealed that they were chemically largely identical. Analysis by energy dispersive X-ray (EDX) spectroscopy indicated the composition Sb_2S_3. The PXRD pattern showed only one broad reflection at $2\theta = 27.3°$ (Cu–$K\alpha_1$ radiation; $d = 326$ pm), implying that the precipitates had very small crystalline domains and were nearly amorphous (Fig. S10†). Yellow-orange amorphous Sb_2S_3 occurs in nature as the mineral metastibnite.[56] Accordingly, the Raman spectrum of the precipitate (Fig. 1) showed a broad signal at 300 cm^{-1} known from metastibnite.[59] As the main signals of antimony sulfide, amorphous and crystalline are below 400 cm^{-1} Raman instead of IR spectroscopy was chosen for sample characterization. The Raman spectrum of the solid obtained from solutions of Sb_2S_3 in $[P_{66614}]Cl$ by precipitation with EtOH (Fig. 1) additionally showed a broad shoulder at 470 cm^{-1} and several overlapping signals from 165 cm^{-1} to 85 cm^{-1}, which could originate from antimony and various sulfur allotropes.

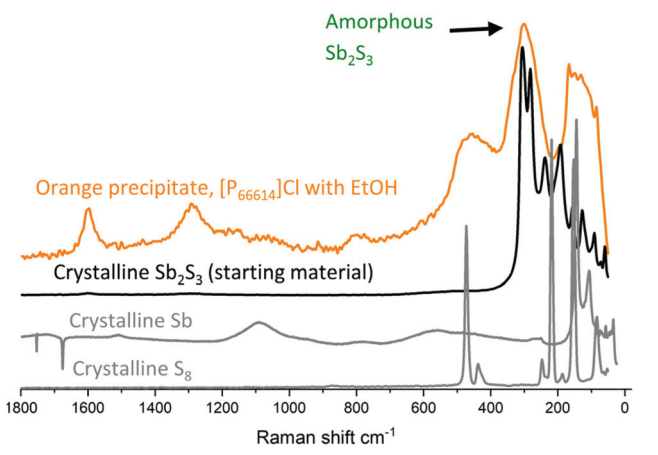

Fig. 1 Comparison of Raman spectra of starting material with the precipitate from solutions of Sb_2S_3 in $[P_{66614}]Cl$ after precipitation with EtOH. The spectra of the amorphous precipitate fits well to the spectra of the crystalline starting material with additional signals for S_8.

The S–S stretching vibration is almost consistent for all sulfur allotropes in the range of 410 cm^{-1} to 480 cm^{-1}. The strong mode of the S–S–S bending vibration around 210 cm^{-1} shifts towards 100 cm^{-1} in larger sulfur molecules (up to S_{20}).[60] Since radical anions of sulfur seem to exist in ILs (see above), complex molecular sulfur chemistry is to be expected. A low intensity signal at about 3000 cm^{-1} (Fig. S4†) can be assigned to C–H modes. Other modes of the IL molecule are less intense and therefore not detectable. Inclusions of IL in the amorphous Sb_2S_3 during the fast precipitation cannot be excluded. However, these cannot be significant amounts since we did not find any corresponding decomposition signals in the DSC. In order to be able to detect possible burning of the samples by the laser, the measurement was repeated several times on the sample. The spectrum and the appearance of the sample did not change significantly.

To explore the effect of air, colored solutions in $[P_{66614}]Cl$, freshly prepared under inert conditions, were diluted with EtOH once in air and the other time under argon atmosphere. In both cases, the orange amorphous precipitate was formed. Scanning electron microscopy (SEM) showed the same fine powder for both, consisting of agglomerates of small spherical particles with fairly uniform diameters of about 10 nm. The particles were charged by the electron beam, resulting in movement of smaller agglomerates. This indicates a low electrical conductivity as can be expected for a colored semiconductor. EDX mapping revealed a homogeneous distribution of antimony and sulfur and a Sb : S ratio of 1 : 1.6 for both the air and the argon sample, corresponding to Sb_2S_3 and possibly some additional sulfur (Fig. S11 and S12†). Traces of phosphorus and chlorine can be attributed to residual IL, which could not be removed even by four washing cycles with EtOH.

Samples of the amorphous precipitates obtained in air or under argon were sealed in small silica ampoules under vacuum for thermal characterization by differential scanning calorimetry (DSC; Fig. 2). Heating to 600 °C at 2 K min^{-1} revealed an exothermic signal at 176 °C (air sample) and 186 °C (argon sample), which can be assigned to crystallization. The endothermic signal at 526 °C (air) or at 538 °C (argon) represents the melting of the samples[20] and is in good agreement with the endothermic signal at 536 °C determined on a sample of crystalline Sb_2S_3 under the same conditions.

Upon cooling, an exothermic double peak at 415 °C (air) and a single signal at 439 °C (argon) marked the recrystallization of the samples. The reference sample of pure Sb_2S_3 solidified at 510 °C. The lowering of the melting point indicates impurities in the two samples obtained from IL, although the level of impurities seems to be higher in the sample precipitated in air. There was no evidence of decomposition of IL molecules that may be present in the sample.

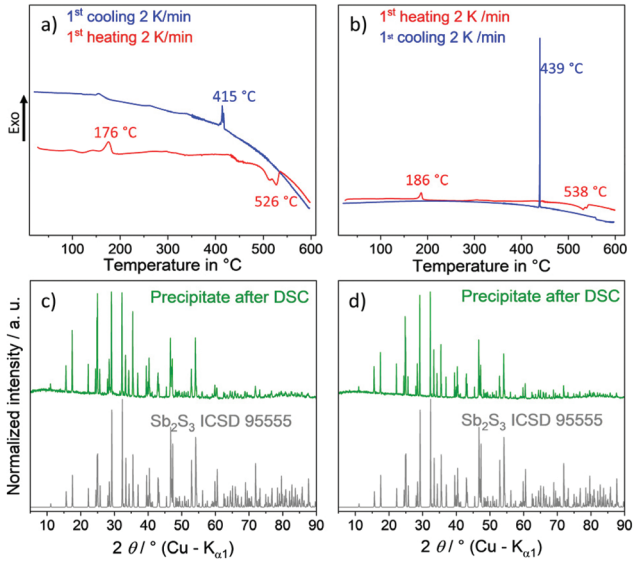

Fig. 2 Comparison of Sb_2S_3 precipitated with EtOH in air (a) and (c) or in argon atmosphere (b) and (d). All temperatures in the DSC (a) and (b) are higher for the in argon precipitated material, where a sharp recrystallization peak at 439 °C occurs. The PXRD patterns (c) and (d) after DSC treatment show both Sb_2S_3 as main phase (simulated from inorganic crystal structure database 95555). The air precipitate shows traces of Sb_2O_3 as impurity.

SEM investigations of the samples after the thermal treatment revealed the typically columns of crystalline stibnite with smaller spherical and irregular shaped particles in between (Fig. 3).

EDX analyses of the crystals confirmed the Sb : S ratio of 1 : 1.50(5) (Table S1†). EDX mapping (Fig. S13 and S14†) underlined the homogenous distribution of the elements and PXRD showed the reflection pattern of Sb_2S_3 in both cases (*cf.* CSD-95555). Traces of Sb_2O_3 were detected in the sample formed in air. It can be assumed that in addition to the oxide, polysulfides and sulfur were also formed by air oxidation, as is known from the chemistry of sulfide in aqueous solution.

In summary, Sb_2S_3 is soluble in $[P_{66614}]Cl$ and $[P_{66614}][OAc]$ at 100 °C, but only slightly. Partly because of the low concentration, it was not possible to identify the species in solution.

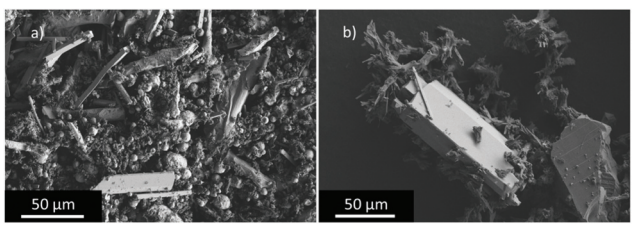

Fig. 3 SEM images of the products from EtOH precipitation after DSC measurements. The precipitate in air (a) shows only few typically columns of Sb_2S_3 in a matrix of irregularly shaped material. In contrast, the precipitate under argon (b) shows larger columns surrounded by dendritic grown material.

There is some evidence suggesting molecular antimony sulfide species in these solutions, possibly similar to the bipyramidal Bi_2S_3 molecule.[50]

Dissolution of Sb_2S_3 in [BMIm]Cl·4.7$AlCl_3$ and formation of the cluster compound $[Sb_{13}S_{16}Cl_2][AlCl_4]_5$

Lewis-acidic imidazolium-based ILs are known to be able to mobilize complex starting materials. In many cases, new inorganic compounds have been crystallized from such solutions. We reacted crystalline Sb_2S_3 with [BMIm]Cl·4.7$AlCl_3$ in a silica ampoule at 160 °C. Controlled cooling to room temperature yielded orange-red, air sensitive, plate-shaped crystals of $[Sb_{13}S_{16}Cl_2][AlCl_4]_5$ in an approximate yield of 60%. EDX analysis of unwashed crystals (Fig. S16, S17 and Table S2†) showed Sb and S in an atomic ratio of 0.80(2), which fits well to the calculated value of 0.8125. The portions of Al and Cl exceeded the expected values due to IL residuals. The crystals appear to survive washing with DCM under inert conditions, as shown by SEM and EDX (Fig. S18 and Table S3†). The ratio determined on washed crystals (in at.%) Sb : S : Cl : Al = 22 (2) : 27(2) : 43(2) : 9(2) nicely agrees with the calculated ratio of 23.3 : 28.6 : 39.3 : 8.9.

X-ray diffraction on a single-crystal at room temperature (Table S4†) revealed a triclinic structure with the space group $P\bar{1}$ (no. 2) and lattice parameters a = 888.86(10) pm, b = 1904.3 (2) pm, c = 2112.5(2) pm, α = 63.884(2)°, β = 80.322(2)°, γ = 88.699(2)° at 296(2) K. Atomic parameters and interatomic distances are listed in Tables S5 and S6.†

The crystal structure (Fig. 4) consists of $[Sb_{13}S_{16}Cl_2]^{5+}$ heteropolycations and $[AlCl_4]^-$ tetrahedra. $[Sb_{13}S_{16}Cl_2][AlCl_4]_5$ is a lighter analogue of $[Sb_{13}Se_{16}Br_2][AlX_4]_5$ (X = $Cl_{0.80(1)}Br_{0.20(1)}$).[47] The cation is a chloride-terminated quadruple-heterocubane formed by 31 atoms (Fig. 5). Its crystallographic symmetry is C_1 but its molecular symmetry is close to C_2, as is the case with the analogous Se–Br compound.[47] The interatomic Sb–S distances can be categorized into primary bonds with bond lengths ranging from 242 to 281 pm and secondary bonds in the range of 298 to 329 pm. The distorted octahedral coordination of the three spiro-antimony atoms combine four primary and two secondary bonds. The terminal antimony atoms have two primary Sb–S bonds and a secondary opposite to the Sb–Cl bond. All other antimony atoms have three primary Sb–S bond. This binding motives are also found in the smaller spiro-double-cubanes of the Se analog $[Sb_7Se_8Br_2]^{3+}$ and $[Sb_7S_8Cl_2]$.[47,49,61] The quadruple-cubane can be seen as an expansion of the double-cubane motive on the terminal, halogenide-terminated antimony with an additional cubane on both sides.[49,52,61–63] As already discussed for the selenium containing double and quadruple-cubanes, this is another example for a postulated oligomerization process. Cubane chains $[Pn_{4+3n}Ch_{4+4n}]^{(4+n)+}$ with n spiro-atoms can be deduced by adding $(Pn_3Ch_4)^+$ moieties to an isolated $[Pn_4Ch_4]^{4+}$ cube.[64–66] Two terminating halide ions, in this case Cl^-, reduce the cluster charge according to the formula $[Pn_{4+3n}Ch_{4+4n}X_2]^{(2+n)+}$, here as a representative of n = 3.[47]

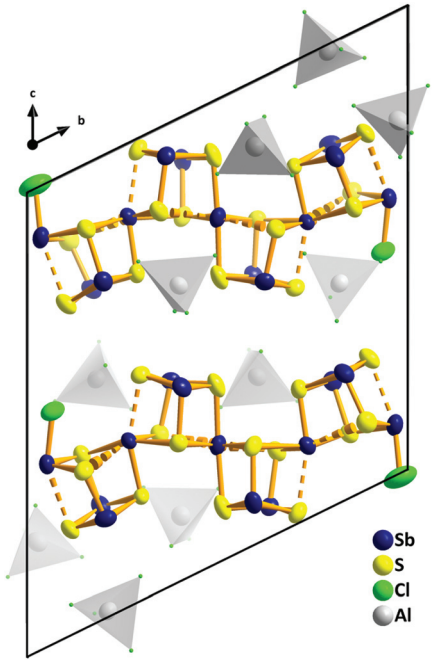

Fig. 4 Crystal structure of $[Sb_{13}S_{16}Cl_2][AlCl_4]_5$ at 296(2) K. $[AlCl_4]^-$ tetrahedra are depicted as polyhedra. The ellipsoids comprise 90% of the probability density of the atoms.

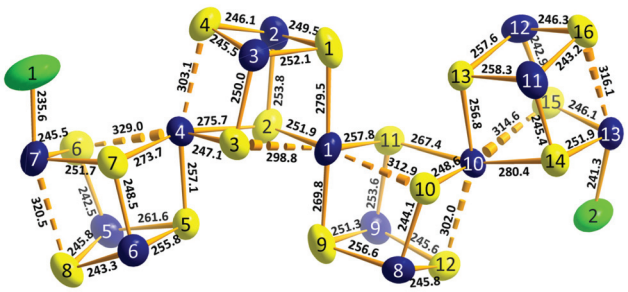

Fig. 5 Quadruple heterocubane cation $[Sb_{13}S_{16}Cl_2]^{5+}$ with bond lengths in pm. The ellipsoids comprise 90% of the probability density of the atoms at 296(2) K.

Conclusions

Our investigations show that both phosphonium ILs, the commercially available $[P_{66614}]Cl$ and the easily accessible $[P_{66614}][OAc]$, are able to dissolve crystalline antimony sulfide at 100 °C. The unknown, presumably uncharged species in solution can be precipitated as amorphous Sb_2S_3 by addition of EtOH or by long-term exposure to air. The amorphous Sb_2S_3 recrystallizes upon annealing. The IL remains intact and can be recycled. The amount of Sb_2S_3 mobilized under the applied conditions is too small for an efficient ionometallurgical processing of the ore. In contrast, Sb_2S_3 readily dissolves in Lewis-acidic imidazolium-based ILs at 160 °C, however, the IL reacts with Sb_2S_3, leading to the precipitation of the cluster compound $[Sb_{13}S_{16}Cl_2][AlCl_4]_5$. These results illustrate two boundary cases of interaction between ILs and Sb_2S_3. For future applications in ore processing, an IL with higher reactivity than the tested phosphonium-based ILs is needed. Targeting a downstream chemistry starting from naturally occurring stibnite, highly reactive imidazolium-based ILs can be an option.

Experimental

The starting materials and the products were handled in an argon-filled glove-box (MBraun UNILab) with $p(O_2)/p^0 < 1$ ppm and $p(H_2O)/p^0 < 1$ ppm. Sb, S, Cu, Ni, Sb_2S_3 (Chempur, >98%) B, Bi, Ge, Mo, Cu, Au, Sn, In, Ti, V, Fe, Co, Ga, Ni, Al, Zn, and Sb (ABCR, 99.999%) were used without further treatment. $AlCl_3$ (Fluka, anhydrous, 98%) was sublimed three times prior to use. DCM (Fisher Scientific, HPLC grade, amylene stabilized) and EtOH (Fisher Scientific, absolute 99.8%, certified AR for analysis) were degassed and dried in an MBraun SPS. $[P_{66614}]Cl$ (>95%, IoLiTec) was dried at 110 °C for 16 h at about 10^{-3} mbar. Further purification (see below) was applied for special purpose. $[P_{66614}][OAc]$ was synthesized by anion metathesis from the chloride IL using K[OAc] according to a literature procedure[10] [BMIm]Cl (98%, Sigma Aldrich) was dried under dynamic vacuum at 100 °C for 16 h.

Synthesis of $[P_{66614}][OAc]$

$[P_{66614}][OAc]$ was synthesized by anion metathesis using potassium acetate and commercial $[P_{66614}]Cl$. 20.8 g of the chloride IL (40 mmol) was dissolved in 20 mL of absolute EtOH, combined under vigorous stirring with 50 mL of an ethanolic solution of potassium acetate (4.9 g, 50 mmol; excess) and stirred for 16 h at room temperature. Precipitated potassium chloride was filtered off. After removal of the solvent on a rotary evaporator, during which more salt precipitated, the IL was filtered again and then dried overnight at 110 °C under dynamic vacuum (about 10^{-3} mbar).

Purification of $[P_{66614}]Cl$

The first step of $[P_{66614}]Cl$ purification was a neutralization of the hydrogen chloride impurities. The IL was stirred with an equivalent volume of 0.1 m NaOH solution for 2 h. Following the separation, the IL phase was washed several times with water. This step might cause foaming during the mixing of IL and water. For the following column chromatography, the IL was adsorbed on silica (Macherey-Nagel, Silica 60 M, 0.04–0.063 mm), which then was dispersed in diethyl ether and filled in the chromatography column. The column (diameter 34 mm) contained 5 cm of the same silica gel dispersed in diethyl ether. The prepared column was eluted with 100 mL diethyl ether. The obtained eluate was rinsed again on the column, which was then eluted again with 200 mL diethyl ether, giving the fraction with the impurities. The subsequent elution with acetonitrile give the fraction with the purified IL. The acetonitrile was removed by vacuum evaporation in a rotary evaporator, and the remaining IL was dried at 110 °C for

16 h under dynamic vacuum (about 10^{-3} mbar). Purity was checked by liquid ^{31}P-NMR spectroscopy.

Synthesis setup

In general, the synthesis in phosphonium ILs were carried out in 5 mL round-bottom flasks equipped with a magnetic stirring bar (PTFE lined, cylindrical, 12.5 mm × 4.5 mm). The flasks were filled with the elements and 1 g of $[P_{66614}]Cl$ under argon atmosphere in a glovebox, sealed with a glass stopper and high-vacuum silicon grease and placed in an oil bath, outside the glovebox. After the mixture had been stirred at the desired temperature for 16 hours, the flask was removed from the bath and cooled to room temperature. Manual separation of the IL was performed in a glovebox using a 1 mL syringe. Supernatant solutions intended for studies on the dissolution behavior of Sb_2S_3 were filtered through a syringe filter (pore width: 0.45 μm). Solid precipitates in synthesis of sulfides, were washed with dried DCM three times. Afterwards the powders were dried in a vacuum drying chamber outside the glovebox at room temperature.

Synthesis of sulfides

The elements were weighted in molar ratio as required for the target phase (in bold):

NiS_2. 1 mmol (58.69 mg) Ni, 2 mmol (64.13 mg) S
Cu_2S. 1.26 mmol (79.85 mg) Cu, 0.63 mmol (20.14 mg) S
CuS. 1.26 mmol (79.85 mg) Cu, 1.26 mmol (40.27 mg) S
Sb_2S_3. 0.5 mmol (60.88 mg) Sb, 0.75 mmol (24.05 mg) S

Dissolution of Sb_2S_3

100 mg or 50 mg of Sb_2S_3 were ground and placed in a 5 mL flask and heated to 100 °C for 16 h. After cooling to room temperature, the solution was removed manually inside a glovebox. For CV measurements 250 mg of Sb_2S_3 were heated in 5 g of $[P_{66614}]Cl$.

Synthesis of $[Sb_{13}S_{16}Br_2][AlCl_4]_5$

The synthesis was carried out in a silica ampoule (length 120 mm, diameter 14 mm). Sb_2S_3 (0.5 mmol, 169.8 mg) was grinded in an agate mortar together with $AlCl_3$ (1.87 mmol, 250 mg) and loaded into the silica ampoule. Upon addition of [BMIm]Cl (0.8 mmol, 70 mg), the reaction mixture began to form a suspension. The reaction mixture in the evacuated and sealed vial was homogenized with a vortex mixer before being placed in a slightly tilted glass tube furnace. The furnace was heated to 160 °C at 5 K min^{-1} and held at this temperature for 44 h. The furnace was then tilted to separate the liquid phase from the solid and cooled to room temperature at 6 K h^{-1}. On the solid side a greyish-black fine powder and orange crystals of $[Sb_{13}S_{16}Br_2][AlCl_4]_5$ had formed.

Powder X-ray diffraction

Characterization of solid reaction products were done by powder X-ray diffraction at 296(1) K on an X'Pert Pro MPD diffractometer (PANalytical), equipped with a curved Ge(111) monochromator, using Cu-Kα_1 radiation (λ = 154.056 pm). For processing and database search (PDF-2021; ICSD Database; PANalytical Example Database) of the powder-patterns the software XPert highscore plus (Version 4.7a). For simulation of powder patterns from single-crystal data (ICSD) the software package STOE WinXPow (Version 2.08) was used.

Single-crystal X-ray diffraction

The orange crystals were manually separated from the powder for single-crystal measurements in glass capillaries. Silicon grease was used to fix the crystals. The capillaries were sealed in a glovebox with an electric burner due to their high sensitivity to air and moisture. Single-crystal X-ray diffraction data was measured at 298(2) K on a four-circle Kappa APEX II CCD diffractometer (Bruker) with a graphite(002)-monochromator and a CCD-detector at T = 296(2) K. Mo-Kα radiation (λ = 71.073 pm) was used. The data were corrected for background, polarization and Lorentz factors using the APEX3 software suite.[67] After integration, a multiscan absorption correction was applied. The structures were solved by direct methods and subsequent difference Fourier analyses. Refinement, including anisotropic displacement parameters for all atoms, was performed against F_o^2 using SHELXL.[68–70] For results see Tables S4 to S6.† The structure was visualized with Diamond.[71] Further details on the crystal structure investigation can be obtained from the Fachinformationszentrum Karlsruhe, 76344 Eggenstein-Leopoldshafen, Germany (fax:+49-7247-808-666; e-mail:crysdata@fiz-karlsruhe.de), or from the Cambridge Crystallographic Data Centre *via* http://www.ccdc.cam.ac.uk/structures, on quoting the depository number CSD 2125501.†

SEM/EDX measurements

Powder samples for SEM/EDX were fixed with a carbon pad to the sample holder. Scanning electron microscopy (SEM) was performed by using an SU8020 instrument (Hitachi) with a triple detector system for secondary and low-energy backscattered electrons (U_e = 2 kV). The compositions of the samples were determined by quantitative EDX (U_e = 30 kV) analysis using an SU8020 instrument (Hitachi) equipped with a Silicon Drift Detector X-Max^N (Oxford).

NMR spectroscopy

For the liquid-state NMR experiments a Bruker Avance Neo 300 MHz spectrometer with a 5 mm high-resolution probe was used. All samples were prepared and sealed with polytetrafluoroethylene caps in low pressure/vacuum 5 mm NMR tubes from Deutero in the glove box under argon atmosphere. Samples of the IL were collected after the solvation of antimony sulfide and filtered, using syringe filters with the pore width 0.45 μm. The filtered ILs were not diluted with a deuterated solvent, instead capillaries filled with DMSO-d6 were added to the IL inside the NMR tube to ensure field-frequency lock. The ^{31}P-NMR spectra were recorded at the transmitter frequency of 121.49 MHz using 128 scans, a relaxation delay of 10 s and a pulse length of 8.3 μs for a 30° pulse. The chemical shifts in the ^{31}P-NMR spectra were referenced relative to H_3PO_4. For the ^{1}H-NMR a 30° pulse with pulse length of

5 μs and a relaxation delay of 1 s was used. For the ^{13}C-NMR a 30° pulse with pulse length of 3.3 μs and a relaxation delay of 5 s was used. The chemical shift of the ^{1}H and ^{13}C NMR spectra are referenced to TMS.

Raman spectroscopy

The spectra were recorded with a Bruker RFS 100 Fourier transform Raman spectrometer. For the 1064 nm excitation light, we used a Nd-YAG-Laser. We used 300 mW for powder samples and 425 mW for liquid samples. Both powder and liquid samples were prepared in capillary glass tubes with a diameter of 1.5 mm. Air sensitive samples were prepare in the glove box under argon atmosphere and the capillary tubes were sealed with modelling clay.

Electrochemical measurements

All electrochemical experiments were performed on a VMP-3 potentiostate form BioLogic controlled by EC-LAB Electrochemistry software. The cyclic voltammogram (CV) was recorded using a three-electrode setup (Wuhan Corrtest Instruments Corp. Ltd). For the measurements 4 mL of the solutions were placed inside a glovebox in the glass container of the electrochemical cell. The cyclic voltammogram (CV) was recorded using a three-electrode setup with a glassy carbon disk working electrode (diameter 3 mm), a platinum wire (Pt, 99.95%, 0.5 mm diameter) as counter electrode and a platinum plate (99.95%, 10 × 10 × 0.1 mm) as pseudo-reference electrode in the range of −3.5 V to 3 V and with a scan rate of 10 mV s^{-1}. Prior to the measurement, the platinum electrodes were rinsed with acetone and cleaned with fuzz-free tissue, before drying on air and moving inside the glovebox. While the measurement the cell was placed in an oil-bath and heated to 100 °C.

Author contributions

Conceptualization by MR. Investigation, data curation, formal analysis, visualization and writing of original draft by MAG and TP. Supervision, project administration, validation, funding acquisition, resources, review and editing by MR and EB.

Conflicts of interest

There are no conflicts to declare.

Acknowledgements

This work was financially supported by the Deutsche Forschungsgemeinschaft (DFG) within the priority program SPP 1708. We thank Prof. Dr Thomas Doert, Maria Herz, Maximilian Knies, and Peng Chen (all TU Dresden) for experimental support and discussions. Open Access funding provided by the Max Planck Society.

Notes and references

1 T. Zhang, T. Doert, H. Wang, S. Zhang and M. Ruck, *Angew. Chem., Int. Ed.*, 2021, **60**, 22148–22165.
2 A. Wolff, J. Pallmann, R. Boucher, A. Weiz, E. Brunner, T. Doert and M. Ruck, *Inorg. Chem.*, 2016, **55**, 8844–8851.
3 T. Zhang, K. Schwedtmann, J. J. Weigand, T. Doert and M. Ruck, *Chem. – Eur. J.*, 2018, **24**, 9325–9332.
4 T. Zhang, T. Doert, H. Wang, S. Zhang and M. Ruck, *Angew. Chem.*, 2021, **133**, 22320–22338.
5 L. H. Finger and J. Sundermeyer, *Chem. – Eur. J.*, 2016, **22**, 4218–4230.
6 J. Guschlbauer and J. Sundermeyer, *ChemistryOpen*, 2021, **10**, 92–96.
7 È. Boros, M. J. Earle, M. A. Gîlea, A. Metlen, A.-V. Mudring, F. Rieger, A. J. Robertson, K. R. Seddon, A. A. Tomaszowska, L. Trusov and J. S. Vyle, *Chem. Commun.*, 2010, **46**, 716–718.
8 A. Wolff, T. Doert, J. Hunger, M. Kaiser, J. Pallmann, R. Reinhold, S. Yogendra, L. Giebeler, J. Sichelschmidt, W. Schnelle, R. Whiteside, H. Q. N. Gunaratne, P. Nockemann, J. J. Weigand, E. Brunner and M. Ruck, *Chem. Mater.*, 2018, **30**, 7111–7123.
9 M. Lê Anh, A. Wolff, M. Kaiser, S. Yogendra, J. J. Weigand, J. Pallmann, E. Brunner, M. Ruck and T. Doert, *Dalton Trans.*, 2017, **46**, 15004–15011.
10 M. A. Grasser, T. Pietsch, E. Brunner, T. Doert and M. Ruck, *ChemistryOpen*, 2021, **10**, 117–124.
11 E. Ahmed, J. Breternitz, M. F. Groh and M. Ruck, *CrystEngComm*, 2012, **14**, 4874.
12 M. F. Groh, S. Paasch, A. Weiz, M. Ruck and E. Brunner, *Eur. J. Inorg. Chem.*, 2015, 3991–3994.
13 J. Richter and M. Ruck, *Molecules*, 2019, **25**, 78.
14 T. Zhang, K. Schwedtmann, J. J. Weigand, T. Doert and M. Ruck, *Chem. Commun.*, 2017, **53**, 7588–7591.
15 A. Söldner, *Deep Eutectic Solvents as Extraction, Reaction and Detection Media for Inorganic Compounds*, Dissertation, University of Regensburg, 2019.
16 T. Zhang, T. Doert and M. Ruck, *Z. Anorg. Allg. Chem.*, 2017, **643**, 1913–1919.
17 J. M. Hartley, C.-M. Ip, G. C. H. Forrest, K. Singh, S. J. Gurman, K. S. Ryder, A. P. Abbott and G. Frisch, *Inorg. Chem.*, 2014, **53**, 6280–6288.
18 E. L. Smith, A. P. Abbott and K. S. Ryder, *Chem. Rev.*, 2014, **114**, 11060–11082.
19 A. C. Rastogi and N. R. Janardhana, *Thin Solid Films*, 2014, **565**, 285–292.
20 A. F. Holleman, E. Wiberg and N. Wiberg, *Lehrbuch der Anorganischen Chemie*, de Gruyter, Berlin, 102 edn, 2007, p. 824.
21 P. T. Anastas, P. Wasserscheid and A. Stark, in *Green Solvents*, ed. P. T. Anastas, A. Stark and P. Wasserscheid, Wiley-VCH, 2013, vol. 6.
22 S. Santner, J. Heine and S. Dehnen, *Angew. Chem., Int. Ed.*, 2016, **55**, 876–893.

23 S. Santner, J. Heine and S. Dehnen, *Angew. Chem.*, 2016, **128**, 886–904.
24 S. Schulz, *Coord. Chem. Rev.*, 2015, **297–298**, 49–76.
25 C. Balischewski, H. S. Choi, K. Behrens, A. Beqiraj, T. Körzdörfer, A. Geßner, A. Wedel and A. Taubert, *ChemistryOpen*, 2021, **10**, 272–295.
26 D. Li and W. Zheng, *Synthetic Inorganic Chemistry*, Elsevier, 2021, pp. 105–128.
27 Y. Lin, D. Xie, W. Massa, L. Mayrhofer, S. Lippert, B. Ewers, A. Chernikov, M. Koch and S. Dehnen, *Chem. – Eur. J.*, 2013, **19**, 8806–8813.
28 B. Peters, G. Stuhrmann, F. Mack, F. Weigend and S. Dehnen, *Angew. Chem., Int. Ed.*, 2021, **60**, 17622–17628.
29 S. Santner, A. Wolff, M. Ruck and S. Dehnen, *Chem. – Eur. J.*, 2018, **24**, 11899–11903.
30 B. Peters, C. Krampe, J. Klärner and S. Dehnen, *Chem. – Eur. J.*, 2020, **26**, 16683–16689.
31 S. Santner, S. Yogendra, J. J. Weigand and S. Dehnen, *Chem. – Eur. J.*, 2017, **23**, 1999–2004.
32 B. Peters, G. Stuhrmann, F. Mack, F. Weigend and S. Dehnen, *Angew. Chem.*, 2021, **133**, 17763–17769.
33 B. Peters, S. Santner and S. Dehnen, *Z. Anorg. Allg. Chem.*, 2020, **646**, 1466–1469.
34 M. Loor, S. Salloum, P. Kawulok, S. Izadi, G. Bendt, J. Guschlbauer, J. Sundermeyer, N. Perez, K. Nielsch, G. Schierning and S. Schulz, *Inorg. Chem.*, 2020, **59**, 3428–3436.
35 M. Loor, G. Bendt, U. Hagemann, C. Wölper, W. Assenmacher and S. Schulz, *Dalton Trans.*, 2016, **45**, 15326–15335.
36 M. Loor, G. Bendt, J. Schaumann, U. Hagemann, M. Heidelmann, C. Wölper and S. Schulz, *Z. Anorg. Allg. Chem.*, 2017, **643**, 60–68.
37 M. Knorr and P. Schmidt, *ChemistryOpen*, 2021, **10**, 125–140.
38 M. Knorr and P. Schmidt, *ChemistryOpen*, 2021, **10**, 57–57.
39 B. Yuan, T. K. Egner, V. Venditti and L. Cademartiri, *Nat. Commun.*, 2018, **9**, 1–7.
40 J. Schaumann, M. Loor, D. Ünal, A. Mudring, S. Heimann, U. Hagemann, S. Schulz, F. Maculewicz and G. Schierning, *Dalton Trans.*, 2017, **46**, 656–668.
41 S. Heimann, S. Schulz, J. Schaumann, A. Mudring, J. Stötzel, F. Maculewicz and G. Schierning, *J. Mater. Chem. C*, 2015, **3**, 10375–10380.
42 E. Ahmed, J. Beck, J. Daniels, T. Doert, S. J. Eck, A. Heerwig, A. Isaeva, S. Lidin, M. Ruck, W. Schnelle and A. Stankowski, *Angew. Chem., Int. Ed.*, 2012, **51**, 8106–8109.
43 E. Ahmed, E. Ahrens, M. Heise and M. Ruck, *Z. Anorg. Allg. Chem.*, 2010, **636**, 2602–2606.
44 E. Ahmed, J. Beck, J. Daniels, T. Doert, S. J. Eck, A. Heerwig, A. Isaeva, S. Lidin, M. Ruck, W. Schnelle and A. Stankowski, *Angew. Chem.*, 2012, **124**, 8230–8233.
45 E. Ahmed, A. Isaeva, A. Fiedler, M. Haft and M. Ruck, *Chem. – Eur. J.*, 2011, **17**, 6847–6852.
46 M. F. Groh, J. Breternitz, E. Ahmed, A. Isaeva, A. Efimova, P. Schmidt and M. Ruck, *Z. Anorg. Allg. Chem.*, 2015, **641**, 388–393.
47 E. Ahmed, J. Breternitz, M. F. Groh, A. Isaeva and M. Ruck, *Eur. J. Inorg. Chem.*, 2014, 3037–3042.
48 M. F. Groh, J. Breternitz, E. Ahmed, A. Isaeva, A. Efimova, P. Schmidt and M. Ruck, *Z. Anorg. Allg. Chem.*, 2015, **641**, 388–393.
49 Q. Zhang, I. Chung, J. I. Jang, J. B. Ketterson and M. G. Kanatzidis, *J. Am. Chem. Soc.*, 2009, **131**, 9896–9897.
50 M. F. Groh, M. Knies, A. Isaeva and M. Ruck, *Z. Anorg. Allg. Chem.*, 2015, **641**, 279–284.
51 M. Knies, M. F. Groh, T. Pietsch, M. Lê Anh and M. Ruck, *ChemistryOpen*, 2021, **10**, 110–116.
52 M. Knies and M. Ruck, *ChemistryOpen*, 2021, **2**, 1–6.
53 M. Green, P. Rahman and D. Smyth-Boyle, *Chem. Commun.*, 2007, 574–576.
54 S. Tyrrell, M. Swadźba-Kwaśny and P. Nockemann, *J. Mater. Chem. A*, 2014, **2**, 2616–2622.
55 S. Tyrrell, G. Behrendt, Y. Liu and P. Nockemann, *RSC Adv.*, 2014, **4**, 36110–36116.
56 A. F. Holleman, E. Wiberg and N. Wiberg, *Lehrbuch der Anorganischen Chemie*, de Gruyter, 102 edn, 2007, p. 544.
57 M. A. Grasser, T. Pietsch, E. Brunner, T. Doert and M. Ruck, *ChemistryOpen*, 2021, **10**, 117–124.
58 M. A. Grasser, T. Pietsch, J. Blasius, O. Hollóczki, E. Brunner, T. Doert and M. Ruck, *Chem. – Eur. J.*, 2022, **28**, e202103770.
59 C. J. Diliegros-Godines, J. Santos Cruz, N. R. Mathews and M. Pal, *J. Mater. Sci.*, 2018, **53**, 11562–11573.
60 B. Eckert and R. Steudel, *Topics in Current Chemistry*, Springer, Berlin, Heidelberg, 2003, pp. 1–116.
61 A. Eich, W. Hoffbauer, G. Schnakenburg, T. Bredow, J. Daniels and J. Beck, *Eur. J. Inorg. Chem.*, 2014, 3043–3052.
62 A. Eich and J. Beck, *Z. Anorg. Allg. Chem.*, 2014, **640**, 2788–2791.
63 A. Eich, S. Schlüter, G. Schnakenburg and J. Beck, *Z. Anorg. Allg. Chem.*, 2013, **639**, 375–383.
64 J. Beck, M. Dolg and S. Schlüter, *Angew. Chem., Int. Ed.*, 2001, **40**, 2287–2290.
65 J. Beck, M. Dolg and S. Schlüter, *Angew. Chem.*, 2001, **113**, 2347–2350.
66 J. Beck, S. Schlüter and N. Zotov, *Z. Anorg. Allg. Chem.*, 2005, **631**, 2450–2456.
67 Bruker, *APEX3 Suite for Crystallographic Software*, Bruker AXS Inc., Madison, Wisconsin, USA, 2017.
68 G. M. Sheldrick, *Acta Crystallogr., Sect. A: Found. Crystallogr.*, 2008, **64**, 112–122.
69 G. M. Sheldrick, *Acta Crystallogr., Sect. C: Struct. Chem.*, 2015, **71**, 3–8.
70 G. M. Sheldrick, *SHELXL, Program for Crystal Structure Refinement – Multi-CPU*, Georg-August-Universität Göttingen, Göttingen, Germany, 2014.
71 K. Brandenburg, *Diamond 4, Crystal and Molecular Structure Visualization*, Crystal Impact GbR, Bonn, Germany, 2017.